



# Mucosal melanomas of different anatomic sites share a common global DNA methylation profile with cutaneous melanoma but show location-dependent patterns of genetic and epigenetic alterations

Philipp Jurmeister<sup>1,2,3,4\*</sup> , Niklas Wrede<sup>2</sup>, Inga Hoffmann<sup>2</sup>, Claudia Vollbrecht<sup>2</sup>, Daniel Heim<sup>2</sup>, Michael Hummel<sup>2,3,4</sup>, Peggy Wolkenstein<sup>3,5</sup>, Ines Koch<sup>2</sup>, Verena Heynol<sup>2</sup>, Wolfgang Daniel Schmitt<sup>2</sup>, Anne Thieme<sup>5</sup>, Daniel Teichmann<sup>5</sup>, Christine Sers<sup>2,3</sup>, Andreas von Deimling<sup>6</sup>, Julia Cara Thierauf<sup>7</sup> , Maximilian von Laffert<sup>2</sup>, Frederick Klauschen<sup>1</sup> and David Capper<sup>3,5</sup>

<sup>1</sup> Institute of Pathology, Ludwig Maximilians University Hospital Munich, Munich, Germany

<sup>2</sup> Institute of Pathology, Charité – Universitätsmedizin Berlin, Corporate Member of Freie Universität Berlin, Humboldt-Universität zu Berlin, Berlin, Germany

<sup>3</sup> German Cancer Consortium (DKTK), Partner Site Berlin, and German Cancer Research Center (DKFZ), Heidelberg, Germany

<sup>4</sup> Berlin Institute of Health (BIH), Berlin, Germany

<sup>5</sup> Charité – Universitätsmedizin Berlin, Corporate Member of Freie Universität Berlin and Humboldt-Universität zu Berlin, Department of Neuropathology, Berlin, Germany

<sup>6</sup> Clinical Cooperation Unit Neuropathology, German Cancer Research Center (DKFZ), German Consortium for Translational Cancer Research (DKTK), Heidelberg, Germany

<sup>7</sup> Department of Pathology, Massachusetts General Hospital/Harvard Medical School, Boston, MA, USA

\*Correspondence to: P Jurmeister, Ludwig Maximilians University Hospital Munich, Institute of Pathology, Thalkirchner Street 36, D-80337 München, Germany. E-mail: philipp.jurmeister@med.uni-muenchen.de

## Abstract

Cutaneous, ocular, and mucosal melanomas are histologically indistinguishable tumors that are driven by a different spectrum of genetic alterations. With current methods, identification of the site of origin of a melanoma metastasis is challenging. DNA methylation profiling has shown promise for the identification of the site of tumor origin in various settings. Here we explore the DNA methylation landscape of melanomas from different sites and analyze if different melanoma origins can be distinguished by their epigenetic profile. We performed DNA methylation analysis, next generation DNA panel sequencing, and copy number analysis of 82 non-cutaneous and 25 cutaneous melanoma samples. We further analyzed eight normal melanocyte cell culture preparations. DNA methylation analysis separated uveal melanomas from melanomas of other primary sites. Mucosal, conjunctival, and cutaneous melanomas shared a common global DNA methylation profile. Still, we observed location-dependent DNA methylation differences in cancer-related genes, such as low frequencies of *RARB* (7/63) and *CDKN2A* promoter methylation (6/63) in mucosal melanomas, or a high frequency of *APC* promoter methylation in conjunctival melanomas (6/9). Furthermore, all investigated melanomas of the paranasal sinus showed loss of *PTEN* expression (9/9), mainly caused by promoter methylation. This was less frequently seen in melanomas of other sites (24/98). Copy number analysis revealed recurrent amplifications in mucosal melanomas, including chromosomes 4q, 5p, 11q and 12q. Most melanomas of the oral cavity showed gains of chromosome 5p with *TERT* amplification (8/10), while 11q amplifications were enriched in melanomas of the nasal cavity (7/16). In summary, mucosal, conjunctival, and cutaneous melanomas show a surprisingly similar global DNA methylation profile and identification of the site of origin by DNA methylation testing is likely not feasible. Still, our study demonstrates tumor location-dependent differences of promoter methylation frequencies in specific cancer-related genes together with tumor site-specific enrichment for specific chromosomal changes and genetic mutations.

© 2021 The Authors. *The Journal of Pathology* published by John Wiley & Sons, Ltd. on behalf of The Pathological Society of Great Britain and Ireland.

**Keywords:** DNA methylation; mucosal melanoma; cutaneous melanoma; uveal melanoma; conjunctival melanoma; DNA sequencing; copy number profiling

Received 23 June 2021; Revised 30 August 2021; Accepted 22 September 2021

*Conflict of interest statement:* David Capper and Andreas von Deimling are listed as inventors on the patent application ‘DNA-methylation based method for classifying tumor species’ (PCT/EP2016/055337) filed by Deutsches Krebsforschungszentrum Stiftung des öffentlichen Rechts and Ruprecht-Karls-Universität Heidelberg. No other conflicts of interest were declared.

## Introduction

The vast majority of malignant melanomas manifest in the skin. However, melanomas can also develop in other organs, such as the uvea and conjunctiva of the eye or the mucosal lining of the respiratory, gastrointestinal, and urogenital tract [1]. Altogether, non-cutaneous melanomas account for approximately 8% of all melanomas [2]. It is well recognized that UV exposure contributes to the development of cutaneous and conjunctival melanoma, and some studies have indicated blue light as a potential underlying cause for uveal melanomas [3–7]. However, the etiology of mucosal melanoma remains uncertain as they occur in body sites that are usually protected from direct sun light [8]. Epidemiologically, patients with cutaneous melanomas tend to be younger, suggesting that older age might play a more important role in the development of non-cutaneous melanoma [9].

Aside from etiological and epidemiological differences, the mutational landscape of non-cutaneous melanomas is also distinct from melanomas of the skin. Several studies have shown that mucosal melanomas are characterized by a relatively low tumor mutational burden [10,11]. *BRAF* mutations occur approximately at the same rates in melanomas originating from the skin and conjunctiva. In contrast, uveal melanomas frequently show *GNAQ*, *GNAI1*, *BAP1*, and *SF3B1* mutations, while *KIT*, *NF1*, and *SF3B1* mutations are more common in mucosal melanomas [10,12–15]. Furthermore, complex numeric and structural alterations are common in mucosal melanomas, recurrently affecting *KIT* and cell cycle-associated genes such as *CDK4* and *CCND1* [10,16–18]. Still, in some instances, the diagnosis of a primary non-cutaneous melanoma can be challenging for pathologists. In particular, if the invasive tumor is not in continuity with a potentially associated melanoma *in situ*, there is no definite histomorphological evidence that can be used to reliably distinguish primary mucosal melanoma from metastatic cutaneous melanoma. The presence of a prototypical *BRAF* V600E mutation, a mutational signature associated with ultraviolet light or high tumor mutational burden may indicate a cutaneous origin of a melanoma when the primary site is unclear, but practical diagnostic value has not been systematically evaluated yet.

Over the last few years, DNA methylation analysis has successfully been used to classify different malignancies, such as tumors of the central nervous system or sarcomas [19–21]. This includes many tumor types that are indistinguishable by currently established diagnostic methods [22,23]. In line with these reports, a recent study described epigenetic differences between cutaneous and uveal melanomas [24]. Apart from its diagnostic value for tumor classification, DNA methylation analysis may also uncover epigenetic changes potentially contributing to tumorigenesis and disease progression, such as promoter hypermethylation and subsequent downregulation or silencing of tumor suppressor genes [25]. In cutaneous and mucosal

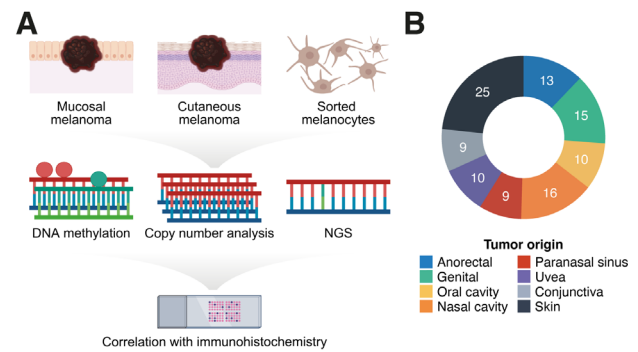


**Figure 1.** Summary of the study design and cohort. (A) Graphical summary of the study design. Samples were subjected to DNA methylation profiling and next generation panel sequencing. Copy number profiles were generated using raw DNA methylation data and differential DNA methylation was calculated comparing tumor samples with normal melanocytes. (B) Pie chart showing the distribution of the sites of tumor origin for the samples included in this study.

melanomas, targeted DNA methylation analysis revealed recurrent hypermethylation of the *PTEN* promoter and described a correlation with worse survival [26].

In the current study, we investigated whether DNA methylation profiling could be used to allocate melanomas to their respective primary site, which would be of great diagnostic value for tumor classification. We performed genome-wide DNA methylation analysis, copy number profiling, and next generation panel sequencing (NGS) in 107 malignant melanoma specimens originating from a variety of anatomical sites (Figure 1A,B). Furthermore, to identify potential epigenetic alterations that might contribute to the development of non-cutaneous melanomas, we compared the DNA methylation profiles of these tumors with normal melanocytes and investigated the effect of the identified changes on staining intensity in immunohistochemistry. Our results show that only uveal melanomas are characterized by a distinct global DNA methylation profile, whereas melanomas from other sites of origin seem to share a common global DNA methylation profile. Further evaluation on the single gene level indicated that in contrast to the shared global profile, mucosal melanomas of different origins are enriched for specific epigenetic and chromosomal alterations in cancer-relevant genes.

## Materials and methods

### Patients and samples

Ethics approval was granted by the local ethics committee of the Charité – University Hospital Berlin (EA1/031/19). A total of 25 cutaneous and 82 non-cutaneous malignant melanoma samples were retrieved from the archives of the Institute of Pathology of the Charité – University Hospital Berlin. The distribution of the various primary sites is shown in Figure 1B. All

samples were re-evaluated by two trained pathologists to confirm the initial diagnosis. Available clinical records were also checked if any doubt regarding the tumor's origin was raised over the course of the disease. This was not the case for any of the cases included in this study. Tumor purity was assessed manually by microscopic inspection using H&E-stained slides. Macrodissection was used to achieve a tumor cell content of at least 60%. All non-cutaneous melanomas were primary tumor samples. For cutaneous melanomas, we exclusively included mucosal metastases of previously diagnosed skin tumors to rule out potential contamination by epidermal cells. For reference, eight aliquots of sorted normal human epidermal melanocytes from two individuals dissolved in RNAlater were obtained from PromoCell (Heidelberg, Germany; C-14040) and subjected to DNA methylation analysis. Additional clinical and histopathological data are available in supplementary material, Table S1.

### Immunohistochemistry

Tissue microarrays were constructed using two cores for each case with a 1.5 mm diameter per core. Immunohistochemical staining was performed on the BenchMark XT (Ventana Medical Systems Inc, Oro Valley, AZ, USA) and the DISCOVERY ULTRA (Ventana) automated slide stainer according to the manufacturer's instructions.

All antibodies were approved for immunohistochemistry by their respective manufacturer. We further evaluated the specificity of all antibodies using an in-house tissue microarray with 25 different normal tissues as well as 20 cancer samples. Rabbit polyclonal APC antibody was obtained from Abcam (Cambridge, UK; catalog number and clone: ab154906). The antibody was used in a 1:500 dilution, based on the manufacturer's instructions as well as previously published investigations [27]. Mouse monoclonal p16 antibody was purchased from Ventana (catalog number: 805-4713; clone: E6H4; dilution: 'ready to use'). Cervical squamous cell carcinoma with known human papilloma virus high-risk infection was used as a positive control. Rabbit monoclonal PTEN antibody was purchased from Cell Signaling Technology (Danvers, MA, USA; catalog number: #9559; clone: 138G6). PTEN staining was done based on the manufacturer's protocol and previously published data; the dilution was adjusted to 1:50 to obtain a stronger signal [28]. Normal tissue was used as a positive control and specificity was tested using endometrial and lung cancer specimens with known deleterious *PTEN* mutations. Rabbit polyclonal RASSF1A antibody was obtained from Abcam (catalog number and clone: ab180801). The staining protocol was based on previously published data; the dilution was adjusted to 1:200 to reduce background staining [29]. Rabbit polyclonal RARB antibody was purchased from Abcam (catalog number and clone: ab53161) and used in a dilution of 1:500 as described in previous studies [30]. Mouse monoclonal antibody to WIF1 was obtained from R&D Systems (Minneapolis,

MN, USA; catalog number: MAB134; clone: 133015) and used in a dilution of 1:100 as previously described [31].

Immunohistochemical analysis was carried out by three trained pathologists who were blinded to any additional information. We calculated an H-score by multiplying the staining intensity (0: no staining; 1: weak staining; 2: moderate staining; 3: strong staining) by the respective percentage of tumor cells, resulting in a value between 0 and 300. The mean of the three independent assessments was used for further analyses.

### DNA extraction

Representative tumor areas were identified using light microscopy of H&E-stained sections. If necessary, macrodissection was performed to reach a tumor cell content of at least 60%. Semi-automated DNA extraction was performed on the Maxwell RSC Instrument (Promega, Madison, WI, USA) using the Maxwell RSC FFPE Plus DNA Purification Kit (AS1720; Promega) for FFPE samples and the Maxwell RSC Blood DNA Kit (AS1400; Promega) for melanocyte specimens, each according to the manufacturer's instructions. Extracted total DNA quantities were measured with a Quantus Fluorometer (Promega) using the QuantiFluor ONE dsDNA Kit (Promega).

### DNA panel sequencing

The Ion AmpliSeq Library Kit 2.0 (Thermo Fisher Scientific, Waltham, MA, USA) was used to perform library preparation of 10 ng of genomic DNA using the Ion AmpliSeq Cancer Hotspot Panel v2 (Thermo Fisher Scientific) covering 50 oncogenes and tumor suppressor genes. Genes and the respective exons covered by the NGS panel are listed in supplementary material, Table S1. Final library was quantified using the Ion Library Quantitation Kit (Thermo Fisher Scientific). Samples were multiplexed and amplified on Ion Sphere Particles with Ion 540 Kit-Chef and were sequenced using Ion 540 Chips on an ION S5 Instrument (Thermo Fisher Scientific). We filtered variants with an allele frequency greater than 1% as determined by the 1000 Genomes Project. Both the Global (AF) and the European (EUR\_AF) populations were evaluated, but identical results were achieved, independent of the selected reference database. Functional annotation was done using publicly available databases (e.g. ClinVar, COSMIC).

### DNA methylation analysis

The Infinium HD FFPE DNA Restore Kit (Illumina, San Diego, CA, USA) was used for DNA restoration of formalin-fixed, paraffin-embedded (FFPE) samples. Subsequently, we used the EpiTect Bisulfite Kit (Qiagen, Hilden, Germany) for bisulfite conversion. DNA methylation analysis was performed using the Infinium MethylationEPIC BeadChip (Illumina) according

to protocols supplied by the manufacturer. BeadArrays were analyzed on an iScan device (Illumina).

Raw DNA methylation data were processed in RStudio (Version 1.2.5019) using the *minfi* package [32,33]. The *pfilter* and *rmSNPandCH* functions from the *wateRmelon* and *DMRcate* packages were used to filter for probes with bad quality, cross-reactivity, and association with SNPs or sex chromosomes [34,35]. Differentially methylated positions (DMPs) and regions (DMRs) were identified using the *dmpFinder* and *DMRcate* function, respectively. DMRs were required to encompass at least four CpG sites with a mean beta fold-change of >0.3 and a false-discovery rate (FDR) less than 0.05. Promoter methylation status was calculated by unsupervised hierarchical clustering on the CpG sites associated with the previously identified DMR. Heatmaps and OncoPrint plots were generated using the *ComplexHeatmap* package [36].

### Copy number analysis

Genome-wide copy number profiling, generation of summary copy number plots, and detection of chromothripsis were carried out using raw DNA methylation data and a modified version of the *conumee* package [37,38]. Unmatched normal tissue which has been analyzed on the same iScan device was used to adjust the baseline. To identify cancer-related candidate genes involved in focal amplifications or deletions, we filtered segment data for sections less than 3 Mbp wide and with a mean deviation of at least 0.4 from the baseline [38,39]. Genes within these segments were annotated using the *getBM* function from the *biomaRt* package [40,41]. Cancer-relevant genes as well as genes known to be involved in fusion events were selected based on the COSMIC Cancer Gene Census [42].

### Statistical analysis

Continuous variables were tested for significance using the Wilcoxon test or the Kruskal–Wallis test for comparisons with more than two categories. Categorical variables were tested for significance using the chi-squared test.

## Results

### Somatic mutations

The most common mutations in mucosal melanomas affected the *NRAS* (7/63; 11%) and *TP53* genes (6/63; 10%). *KIT* mutations were present in three mucosal melanoma specimens (5%). *BRAF* mutations were common in cutaneous (9/25; 36%) and conjunctival (7/9; 78%) melanomas but occurred in only two mucosal melanoma samples (2/63; 3%). Furthermore, we observed *GNAQ* or *GNAI1* mutations in 60% (6/10) of uveal melanomas. The most important mutations are summarized in Figure 2A; a complete list of somatic variants is presented in supplementary material, Table S2.

### Copy number variations

Overall, focal copy number changes were frequent events in mucosal and also cutaneous melanomas but were considerably rarer in conjunctival melanomas. Uveal melanomas commonly showed recurrent arm-level alterations such as gain of chromosome 8q, while focal copy number changes were exceedingly rare. In line with these results, we observed signs of chromothripsis in 41% (26/63) of mucosal melanomas compared with a rate of 11% (1/9) and 16% (4/25) in melanomas of the conjunctiva and the skin, respectively (Figure 2A). Summary copy number plots for the different anatomic locations are shown in supplementary material, Figure S1.

We identified four hotspot regions with recurrent focal amplifications enriched in mucosal melanoma samples, including the cytobands 4q11–12, 5p15, 11q13–14, and 12q14–15. While 33 of 63 mucosal melanoma samples (52%) showed focal amplification in at least one of these regions, these alterations were significantly less common in conjunctival (1/9; 11%;  $p = 0.049$ ) and cutaneous melanomas (3/25; 12%;  $p = 0.001$ ) and did not occur in uveal melanomas (0/10;  $p = 0.005$ ). The distribution of these chromosomal alterations according to primary site is summarized in Figure 2B and also listed in Table 1.

Sixteen mucosal melanomas (25%) and one conjunctival melanoma showed focal amplifications of the 4q11–12 gene locus (Figure 2C). This resulted in focal gains of cancer-related genes such as *KDR* (24%), *KIT* (24%), and *PDGFRA* (19%). Focal amplification of 5p15 (Figure 2D) was mainly observed in melanomas of the oral cavity (8/10; 80%) and usually occurred in combination with additional, complex deletions and amplifications on chromosome 5p. In all cases, this resulted in focal amplification of the *TERT* gene locus.

Focal amplification of 11q13–14 (Figure 2E) affecting the *CCND1* or *GAB2* gene occurred in 14 tumors and mainly affected mucosal melanomas of the nasal cavity (9/16; 56%).

12q14–15 amplification (Figure 2F), involving cancer-related genes such as *CDK4* and *PTPRB*, was present in six mucosal melanoma samples and was evenly distributed among melanomas of the anorectum, the genital region, the oral cavity, and the nasal cavity. Furthermore, focal amplification also occurred in one cutaneous melanoma.

With regard to focal deletions, loss of *CDKN2A/B* and *LARP4B* frequently occurred in both mucosal (16/36; 25% and 12/63; 19%) and cutaneous melanomas (7/25; 28% and 3/25; 12%) but not in uveal melanomas (0/10; 0%).

### DNA methylation

Using unsupervised hierarchical clustering, uveal melanomas and normal melanocytes formed separate clusters (Figure 3A). However, there was no separation between mucosal, conjunctival, and cutaneous melanomas by their global DNA methylation profile. Furthermore, the results from unsupervised clustering were not biased



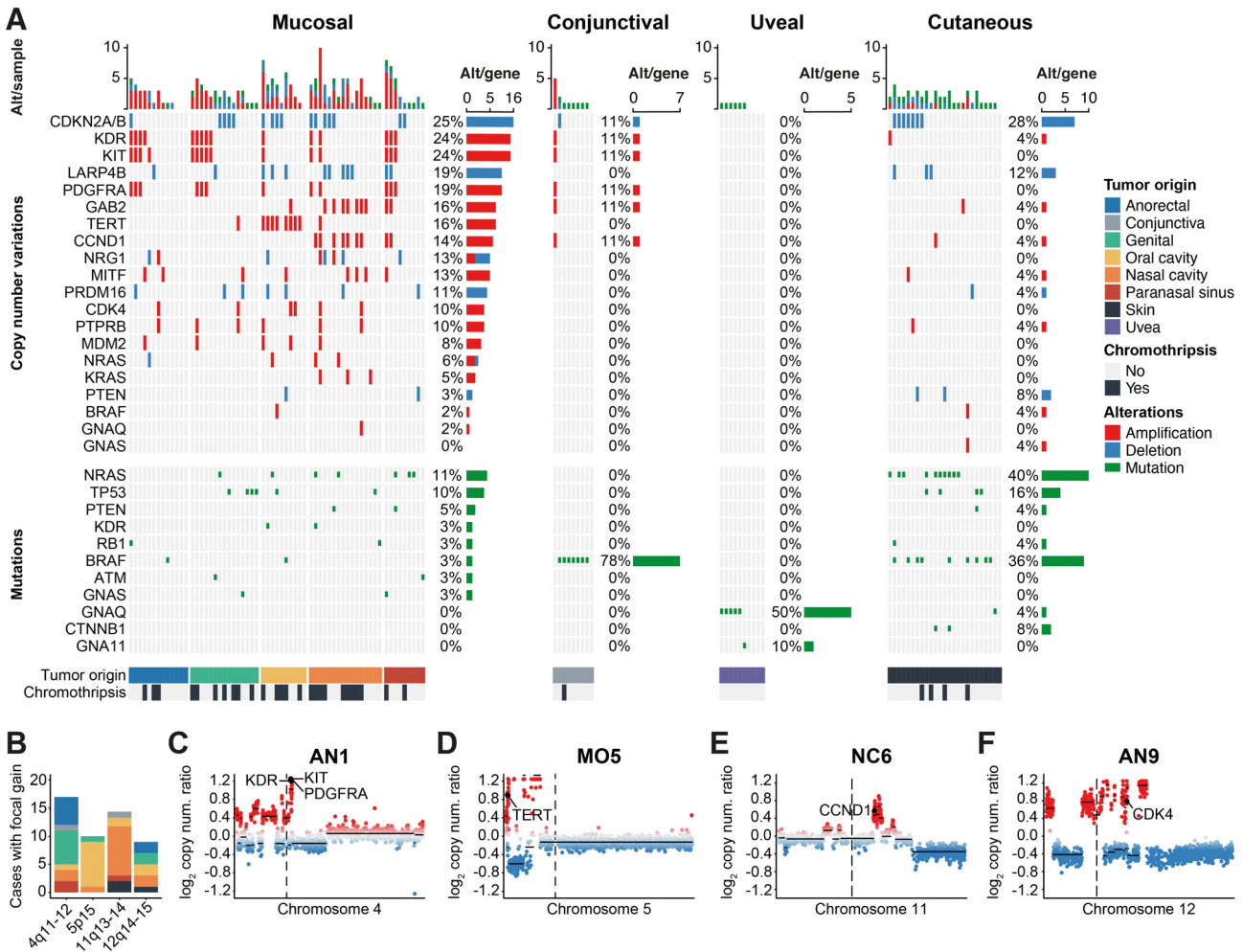


**Figure 2.** Results from next generation DNA panel sequencing and copy number analysis. (A) OncoPrint plot summarizing the most frequent mutations and focal copy number changes in mucosal, ocular, and cutaneous melanomas. The alteration type is annotated by color. Bar plots on the top represent the sum of all alterations per sample (Alt/sample) and bar plots on the right show the number of alterations per gene (Alt/gene), including the percentage. Annotation bars at the bottom of the OncoPrint plots annotate the exact melanoma primary site and whether signs of chromothripsis have been detected. (B) Stacked bar plots showing the relationship between four hotspot gene loci harboring recurrent focal copy amplifications and the tumor origin of the affected samples. (C–F) Detailed copy number plots showing examples for cases with focal amplifications of the 4q11–12 (C), 5p15 (D), 11q13–14 (E), and 12q14–15 (F) gene locus. The annotation highlights associated and recurrently amplified cancer-relevant genes. The headings correspond to the case ID provided in supplementary material, Table S3 (AN, anorectal; MO, oral cavity; NC, nasal cavity).

by other covariates such as sex, age, tumor purity or tumor pigmentation. Comparable results were seen using dimensionality reduction methods such as uniform manifold approximation and projection (UMAP) as well as t-distributed stochastic neighbor embedding (t-SNE; supplementary material, Figure S2).

We performed a group-wise differential methylation analysis comparing cutaneous melanomas with non-cutaneous melanomas of different anatomical sites to quantify the epigenetic similarities or differences between these groups. In accordance with the results from unsupervised cluster analysis, differential methylation analysis revealed high rates of differentially methylated positions (DMPs) and differentially methylated regions (DMRs) between cutaneous and uveal melanomas (Figure 3B), whereas differences between cutaneous melanomas and mucosal melanomas were less prominent. We observed the highest rates of DMPs and

DMRs between cutaneous melanomas and tumors arising from the paranasal sinus, followed by the anorectum, the nasal cavity, and the conjunctiva. Melanomas from the genital region and the oral cavity showed very few or even no differential methylation when compared with cutaneous melanomas.

Further, to demonstrate potential cancer-specific epigenetic modifications, we compared our tumor samples with normal melanocytes. Across primary sites, there was a variable number of DMPs, ranging from 102 292 in anorectal melanoma to 510 124 in melanomas of the oral cavity. Focusing on the 1000 most significant DMPs, we saw little overlap between the different primary sites (supplementary material, Figure S3A). Furthermore, we observed a significantly different genomic CpG annotation (promotor-associated versus gene body versus intergenic) in relation to the melanoma primary tumor site (supplementary material, Figure S3B). The majority of

Table 1. The genetic or epigenetic alterations enriched in the respective site of origin.

	Cutaneous	Anorectal*	Genital*	Nasal cavity*	Oral cavity*	Paranasal sinus*	Conjunctiva	Uvea	
Mutations	<i>BRAF</i>	-	-	-	-	-	<i>BRAF</i>	<i>GNAQ</i> , <i>GNA11</i>	
CNP	-	High rate of focal copy number changes, chromothripsis						-	Whole-arm alterations
Focal CNV	-	4q11-12, 12q14-15	4q11-12, 12q14-15	4q11-12, 11q13-14, 12q14-15	4q11-12, 5p15, 12q14-15	4q11-12, 12q14-15	-	-	
DNA methylation	<i>CDKN2A</i> , <i>RARB</i>	-	<i>RASSF1</i>	-	<i>RARB</i>	<i>PTEN</i> , <i>RASSF1</i>	<i>CDKN2A</i> (p16), <i>APC</i>	<i>RASSF1</i>	

CNP, copy number profile; CNV, copy number variations.

\*High rate of focal copy number changes, chromothripsis.

the most significant CpG sites in melanomas of the conjunctiva (44%;  $p < 0.001$ ), the paranasal sinus (41%;  $p < 0.001$ ), the skin (39%;  $p < 0.001$ ), and the nasal cavity (37%;  $p = 0.001$ ) were located in promoter regions. On the other hand, this was only rarely observed in uveal melanomas (14%;  $p < 0.001$ ), which mainly showed differential methylation in the gene body region (45%;  $p < 0.001$ ). Notably, the 1000 most significant DMPs showed very little overlap between different melanoma primary sites.

The results were filtered for DMRs associated with cancer-related genes and regulatory sequences. The results are summarized in Figure 3C,D. Overall, uveal melanomas rarely showed promoter methylation of cancer-relevant genes, with the exception of high rates of *RASSF1* promoter methylation (8/10; 80%). For all other primary sites, we observed comparable rates of *WIF1* (33–57%) and *RASSF1* (44–51%) promoter methylation. Methylation of the *PTEN* promoter was enriched in mucosal melanomas of the paranasal sinus (8/9; 89%). Interestingly, the only paranasal sinus specimen with a non-methylated promoter showed a *PTEN* deletion. Furthermore, methylation of the *CDKN2A* promoter region associated with the p16 transcript was relatively rare in mucosal melanomas (6/63; 10%) compared with cutaneous (9/25; 36%) and conjunctival (4/9; 44%) melanomas, and did not occur in mucosal melanomas arising from the nasal cavity, the paranasal sinus, or the oral cavity. Promoter methylation of the *APC* gene was most common in conjunctival melanomas (6/9; 67%) but also occurred in cutaneous (7/25; 28%) and mucosal melanomas (8/63; 13%). Recurrently altered promoter methylation in relation to the primary site is also summarized in Table 1.

Gene set enrichment analysis of the results from differential methylation analysis revealed that all anatomical sites were enriched for receptor tyrosine kinase signaling (supplementary material, Figure S4). Other enriched ontologies included WNT signaling (anorectal and genital mucosal melanoma), MAPK signaling (anorectal, conjunctival, and uveal melanoma) and PI3K/AKT signaling (oral cavity and uveal melanoma). Genes associated with keratinization were only overrepresented in cutaneous melanoma.

### Correlation with immunohistochemical staining intensity

As described in the sections on copy number variations and DNA methylation, for *CDKN2A* (p16) and *PTEN* we

observed both focal gene deletions and gene promoter methylation. These alterations were observed in an exclusive manner. Both alterations were associated with strongly reduced or complete loss of protein expression (Figure 4A, B). Furthermore, promoter methylation of the *RARB*, *RASSF1*, *APC*, and *WIF1* promoters was associated with significantly reduced immunohistochemical staining intensity of their related proteins (Figure 4C–F).

### Discussion

With this study, we provide the most comprehensive epigenetic study of non-cutaneous melanomas to date. In addition to DNA methylation analysis, we also integrated copy number analysis and DNA mutational profiling and assessed associations of these alterations with immunohistochemical staining intensity. Our data show that uveal melanomas have a highly distinct global DNA methylation pattern, whereas mucosal and conjunctival melanomas share a global epigenetic pattern with cutaneous melanomas. A more focused approach indicated that primary tumor sites differ in the frequencies of promoter methylation at specific cancer-related genes and show different patterns of copy number changes. The observed differences are summarized in Table 1.

In line with previous reports, DNA panel sequencing revealed high rates of *BRAF* mutations in cutaneous and conjunctival melanoma, as well as frequent *GNAQ* and *GNA11* mutations in uveal melanoma samples [12,13]. Regarding mucosal melanoma, we observed expected frequencies of *NRAS* and *TP53* mutations, while *KIT* mutations were relatively uncommon compared with other studies [10,14,15]. As described previously, *BRAF* mutations were rare in mucosal melanomas and only affected two samples. Both *BRAF* mutations did not affect codon 600 and there is conflicting information as to whether these patients might benefit from BRAF/MEK inhibition [43,44]. Furthermore, the frequency of *GNAQ* and *GNA11* mutations in our study was slightly lower than expected. This could be due to the fact that the NGS panel that was used for our investigation only covers mutations in exon 5 and would therefore miss rarer alterations in other exons (e.g. exon 4). The reported frequency of *GNAQ* and *GNA11* mutations should therefore be interpreted with some caution.

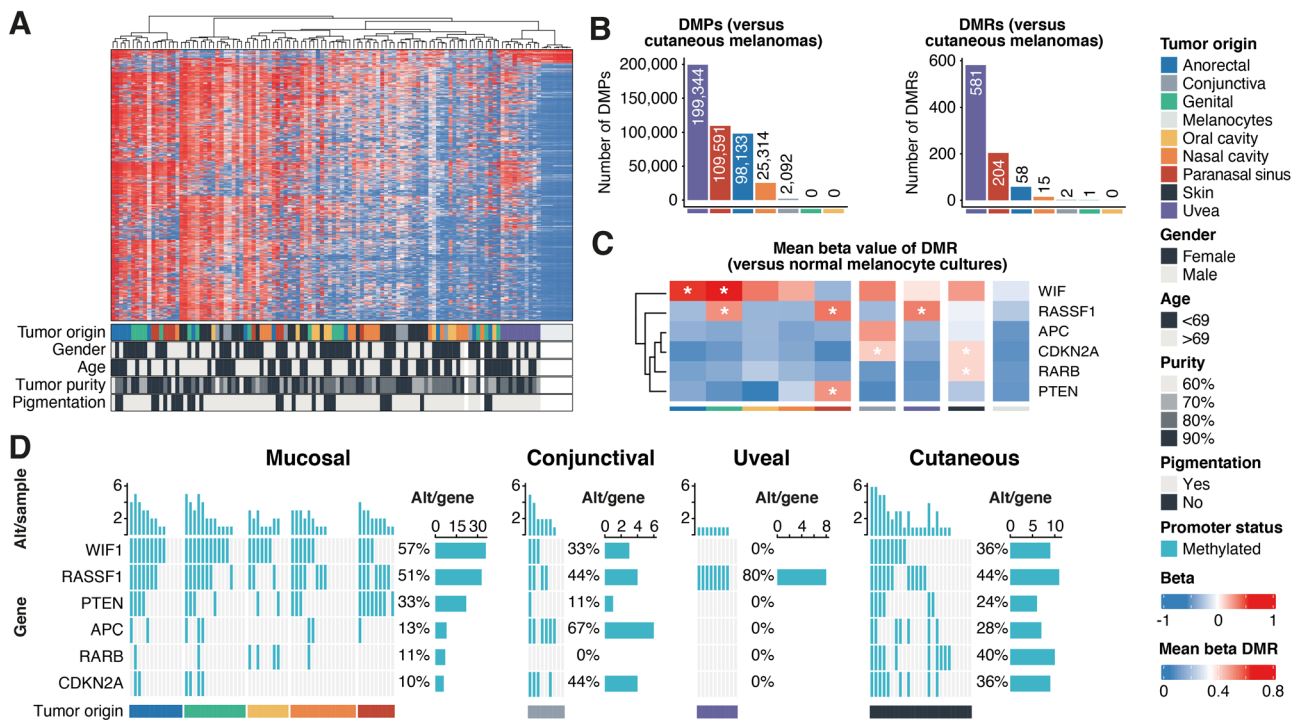


**Figure 3.** Summary of the results from DNA methylation analysis. (A) Unsupervised hierarchical cluster analysis using the 2000 most variant CpG sites. The melanoma site of origin as well as potential confounders is annotated below. (B) Bar plots showing the number of differentially methylated positions (DMPs) and regions (DMRs) between cutaneous and non-cutaneous melanomas. (C) Heatmap showing the results from differential methylation region analysis comparing normal melanocytes and the different sites of origin. Columns correspond to the melanoma primary site, as defined by the annotation bar below the plot. Rows correspond to cancer-relevant genes. The heatmap colors show the mean beta fold-change of the differentially methylated region in the promoter of the respective gene. Asterisks indicate genes with significant differential DNA methylation. (D) OncoPrint plot showing the promoter methylation status of selected cancer-relevant genes for the different sites of melanoma origin.

Copy number analysis revealed high rates of focal copy number changes and high rates of chromothripsis in mucosal melanoma samples, including focal amplifications in four hotspot regions on chromosomes 4q, 5p, 11q, and 12q, which is in line with previous investigations [45–47]. Two recent whole-genome sequencing studies were able to associate amplifications in these regions with structural rearrangements [10,48]. Also in line with these reports, we observed that focal amplification of *TERT* at the 5p15 gene locus primarily occurred in tumors of the oral cavity [49]. Furthermore, we observed that 11q13–14 amplification was enriched in melanomas of the nasal cavity, which has not previously been reported. This might be due to the fact that most previous investigations studied mucosal melanomas of the paranasal sinus and nasal cavity combined as one group and did not investigate them separately.

Previous studies suggested that alterations of cell cycle-related genes play a major role in mucosal melanomas [10,16]. We observed chromosomal or epigenetic alteration of at least one gene associated with the CDK4/6 pathway (*CCND1*, *CDKN2A*, *CDK4*, *RB1*) in more than half of all the mucosal melanoma specimens. This provides further evidence that a fraction of patients with mucosal melanoma could profit from treatment with CDK4/6 inhibitors [10,48,50].

Over the last few years, various studies have shown that DNA methylation signatures can be used to assign different tumors to their tissue origin with previously unmatched

accuracy [19,21–23,38]. Although we investigated melanomas from a variety of primary sites, only uveal melanomas were assigned to a distinct global cluster using unsupervised cluster analysis. The degree of similarity between mucosal melanomas and cutaneous melanomas seems to depend on the respective site of origin: mucosal melanomas of the anorectum, the paranasal sinus, and the nasal cavity show some differential methylation, while tumors of the genital region, the oral cavity, and the conjunctiva show very little or virtually no differences to melanomas of the skin. While DNA methylation could thus be used to differentiate uveal melanomas from other primary sites, this approach does not seem suitable for distinguishing mucosal, conjunctival, and cutaneous melanomas. Griewank *et al* previously reported remarkable molecular similarities between leptomeningeal melanocytic tumors, uveal melanomas, and blue nevus-like melanomas, including a shared global DNA methylation pattern [24]. Based on this study and our results, one could hypothesize that mucosal, conjunctival, and cutaneous melanomas share a common progenitor cell that is distinct from melanocytes that give rise to leptomeningeal melanocytic tumors, uveal melanomas, and blue nevus-like melanomas.

Our findings further indicate that differences in UV exposure between different melanoma primary sites do not result in global DNA methylation changes. This contrasts with the higher tumor mutational burden observed in cutaneous melanomas which is usually attributed to UV exposure [10].



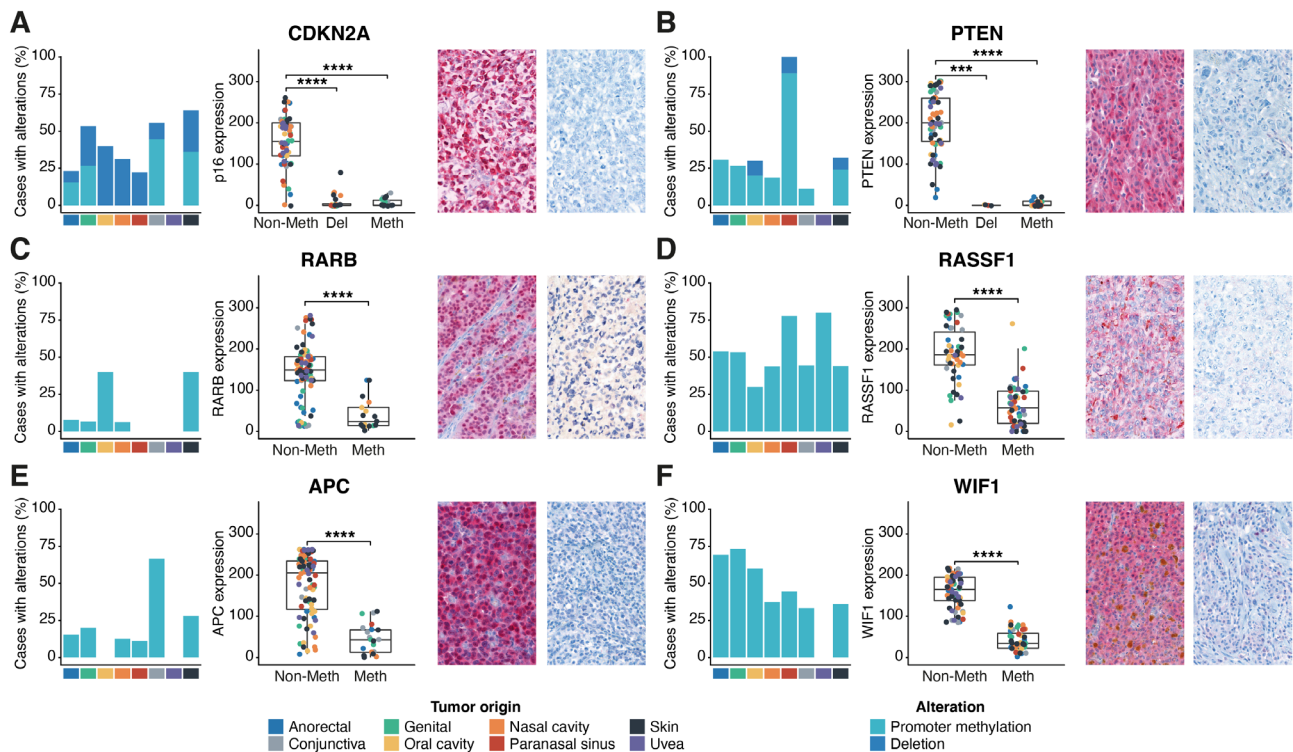


**Figure 4.** Association of epigenetic changes and chromosomal alterations with immunohistochemical staining intensity. (A–F) Bar charts on the left show the rate of alterations according to the primary site, which is indicated by the colored annotation bar below the plot. Combined box and dot plots show the H-score staining intensity levels of the respective proteins for tumors with non-methylated (non-Meth) promoter and copy number status compared with specimens with promoter methylation (Meth) or deletion (Del). The color of the dots corresponds to the melanoma primary site of each individual case. The panels on the right show examples of immunohistochemical stains of positive and negative cases. Levels of significance: \*\*\* $p \leq 0.001$ , \*\*\*\* $p \leq 0.0001$ .

At the single gene level, we were able to confirm previously described recurrent promoter hypermethylation of cancer-related genes in cutaneous melanomas, such as *RASSF1*, *RARB*, and *CDKN2A* [51–53]. In line with the global differences between uveal melanomas and other melanoma primary sites, *RARB* and *CDKN2A* were not affected by hypermethylation in the uveal melanoma specimens included in our study, confirming previous reports [54]. The only exception to this was a high rate of *RASSF1* promoter hypermethylation, which has already been described to be regularly affected [55]. These data suggest that aberrant promoter methylation may be less crucial in the development of uveal melanomas compared with melanomas of other primary sites. Still, numerous studies have shown that DNA methylation can be used for risk stratification in uveal melanoma patients, suggesting a central role in disease progression [56–58]. Overall, the role of DNA methylation in the development of uveal melanomas requires additional research, including functional studies.

Despite the global similarities between cutaneous and mucosal melanomas, we observed some differences in the promoter methylation status of cancer-related genes. Remarkably, all melanomas of the paranasal sinus showed loss of *PTEN* positivity in immunohistochemistry, most likely due to promoter methylation in the majority of cases. Our results indicate that epigenetic silencing of *PTEN* is likely an important step in the development of melanomas of the paranasal sinus. Our

findings are supported by a case report [59]. A previous study investigating *PTEN* promoter methylation in a larger cohort of mucosal melanomas unfortunately did not report their exact primary sites [26].

A potential limitation of our study is that we solely used immunohistochemistry for the estimation of protein expression instead of possibly more precise and quantitative methods such as western blotting or mass spectrometry-based proteomics. Although we observed reasonable relationships between the promoter methylation status and the immunohistochemical staining intensity, this does not necessarily correlate with the actual protein expression levels.

In summary, our results show distinct epigenetic signatures in uveal melanomas and remarkable similarities between the DNA methylation profiles of melanomas originating from the skin, the conjunctival lining, and the mucosal lining. Although DNA methylation alone is not sufficient to distinguish mucosal, conjunctival, and cutaneous melanoma, the different rates of genetic, chromosomal, and epigenetic alterations combined could still be useful for identifying the most likely primary site.

## Acknowledgements

We gratefully acknowledge the expert technical assistance of Sylwia Handzik, Ulrike Stötzer, Barbara Meyer-Bartell, and Manuela Pacyna-Gengelbach. We thank Damian



Stichel for providing a modified version of the *conumee* package to generate frequency copy number profiles. Parts of Figure 1 were created with BioRender.com. This project was supported by the Berliner Krebsgesellschaft (JUFF201917) to PJ and DC. PJ is a participant in the Berlin Institute of Health (BIH) Charité Digital Clinician Scientist Program funded by the Charité – Universitätsmedizin Berlin, the Berlin Institute of Health, and the German Research Foundation (DFG).

### Author contributions statement

PJ, CT and DC were responsible for the conceptualization of the investigation. Data were curated by PJ, JT and DC. The formal analysis was performed by PJ, CV and DH. Funding was provided by PJ and DC. The investigation was performed by PJ, IH, NW, CV, PW, IK, VH, DT, MvL and JT. The methodology was developed by PJ. The project was administered by PJ and DC. Resources were provided by ET, MH, WDS, CS, DC, AvD, MvL, FK and DC. The software was written by PJ, DH and AT. The project was supervised by PJ and DC. Validation was performed by PJ. Visualizations were created by PJ and DH. Writing of the original draft was done by PJ and DC. All the authors contributed to the final review and editing of the manuscript.

### Data availability statement

Raw DNA methylation data have been deposited in GEO under the accession number GSE178416 (<https://www.ncbi.nlm.nih.gov/geo/query/acc.cgi?acc=GSE178416>). Relevant somatic mutations are summarized in supplementary material, Table S2. The study protocol that has been approved by the local ethics committee does not permit permanent deposition of mutational sequencing data from retrospective patient series. Raw sequencing data will therefore only be shared upon reasonable request.

### References

- Mihajlovic M, Vlajkovic S, Jovanovic P, *et al.* Primary mucosal melanomas: a comprehensive review. *Int J Clin Exp Pathol* 2012; **5**: 739–753.
- Patrick RJ, Fenske NA, Messina JL. Primary mucosal melanoma. *J Am Acad Dermatol* 2007; **56**: 828–834.
- Rivolta C, Royer-Bertrand B, Rimoldi D, *et al.* UV light signature in conjunctival melanoma; not only skin should be protected from solar radiation. *J Hum Genet* 2016; **61**: 361–362.
- Krantz BA, Dave N, Komatsubara KM, *et al.* Uveal melanoma: epidemiology, etiology, and treatment of primary disease. *Clin Ophthalmol* 2017; **11**: 279–289.
- Pane AR, Hirst LW. Ultraviolet light exposure as a risk factor for ocular melanoma in Queensland, Australia. *Ophthalmic Epidemiol* 2000; **7**: 159–167.
- Lutz JM, Cree I, Sabroe S, *et al.* Occupational risks for uveal melanoma results from a case–control study in nine European countries. *Cancer Causes Control* 2005; **16**: 437–447.
- Logan P, Bernabeu M, Ferreira A, *et al.* Evidence for the role of blue light in the development of uveal melanoma. *J Ophthalmol* 2015; **2015**: 386986.
- Tyrrell H, Payne M. Combatting mucosal melanoma: recent advances and future perspectives. *Melanoma Manag* 2018; **5**: MMT11.
- Chang AE, Karnell LH, Menck HR. The National Cancer Data Base report on cutaneous and noncutaneous melanoma: a summary of 84,836 cases from the past decade. The American College of Surgeons Commission on Cancer and the American Cancer Society. *Cancer* 1998; **83**: 1664–1678.
- Newell F, Kong Y, Wilmott JS, *et al.* Whole-genome landscape of mucosal melanoma reveals diverse drivers and therapeutic targets. *Nat Commun* 2019; **10**: 3163.
- Johnson DB, Carlson JA, Elvin JA, *et al.* Landscape of genomic alterations (GA) and tumor mutational burden (TMB) in different metastatic melanoma (MM) subtypes. *J Clin Oncol* 2017; **35**: 9536.
- Griewank KG, Westekemper H, Murali R, *et al.* Conjunctival melanomas harbor *BRAF* and *NRAS* mutations and copy number changes similar to cutaneous and mucosal melanomas. *Clin Cancer Res* 2013; **19**: 3143–3152.
- Shoushtari AN, Carvajal RD. GNAQ and GNA11 mutations in uveal melanoma. *Melanoma Res* 2014; **24**: 525–534.
- Hintzsche JD, Gorden NT, Amato CM, *et al.* Whole-exome sequencing identifies recurrent *SF3B1* R625 mutation and comutation of *NFI* and *KIT* in mucosal melanoma. *Melanoma Res* 2017; **27**: 189–199.
- Nassar KW, Tan AC. The mutational landscape of mucosal melanoma. *Semin Cancer Biol* 2020; **61**: 139–148.
- Lyu J, Song Z, Chen J, *et al.* Whole-exome sequencing of oral mucosal melanoma reveals mutational profile and therapeutic targets. *J Pathol* 2018; **244**: 358–366.
- Hayward NK, Wilmott JS, Waddell N, *et al.* Whole-genome landscapes of major melanoma subtypes. *Nature* 2017; **545**: 175–180.
- Wong K, van der Weyden L, Schott CR, *et al.* Cross-species genomic landscape comparison of human mucosal melanoma with canine oral and equine melanoma. *Nat Commun* 2019; **10**: 353.
- Capper D, Jones DTW, Sill M, *et al.* DNA methylation-based classification of central nervous system tumours. *Nature* 2018; **555**: 469–474.
- Koelsche C, Hartmann W, Schrimpf D, *et al.* Array-based DNA-methylation profiling in sarcomas with small blue round cell histology provides valuable diagnostic information. *Mod Pathol* 2018; **31**: 1246–1256.
- Koelsche C, Schrimpf D, Stichel D, *et al.* Sarcoma classification by DNA methylation profiling. *Nat Commun* 2021; **12**: 498.
- Jurmeister P, Bockmayr M, Seegerer P, *et al.* Machine learning analysis of DNA methylation profiles distinguishes primary lung squamous cell carcinomas from head and neck metastases. *Sci Transl Med* 2019; **11**: eaaw8513.
- Jurmeister P, Schöler A, Arnold A, *et al.* DNA methylation profiling reliably distinguishes pulmonary enteric adenocarcinoma from metastatic colorectal cancer. *Mod Pathol* 2019; **32**: 855–865.
- Griewank K, Koelsche C, van de Nes JAP, *et al.* Integrated genomic classification of melanocytic tumors of the central nervous system using mutation analysis, copy number alterations, and DNA methylation profiling. *Clin Cancer Res* 2018; **24**: 4494–4504.
- Ng JM, Yu J. Promoter hypermethylation of tumour suppressor genes as potential biomarkers in colorectal cancer. *Int J Mol Sci* 2015; **16**: 2472–2496.
- Roh MR, Gupta S, Park KH, *et al.* Promoter methylation of *PTEN* is a significant prognostic factor in melanoma survival. *J Invest Dermatol* 2016; **136**: 1002–1011.
- Wang W, Shao F, Yang X, *et al.* METTL3 promotes tumour development by decreasing APC expression mediated by APC mRNA N<sup>6</sup>-methyladenosine-dependent YTHDF binding. *Nat Commun* 2021; **12**: 3803.

28. Trovato F, Parra R, Pracucci E, *et al.* Modelling genetic mosaicism of neurodevelopmental disorders *in vivo* by a Cre-amplifying fluorescent reporter. *Nat Commun* 2020; **11**: 6194.
29. Chen T, Sun Z, Liu F, *et al.* RASSF1A and SIRT6 in non-small cell lung cancer: relationship with clinical outcome. *Oncol Lett* 2017; **14**: 5759–5764.
30. Liu CH, Raj S, Chen CH, *et al.* HLA-B27-mediated activation of TNAP phosphatase promotes pathogenic syndesmophyte formation in ankylosing spondylitis. *J Clin Invest* 2019; **129**: 5357–5373.
31. Kawakami K, Hirata H, Yamamura S, *et al.* Functional significance of Wnt inhibitory factor-1 gene in kidney cancer. *Cancer Res* 2009; **69**: 8603–8610.
32. Aryee MJ, Jaffe AE, Corrada-Bravo H, *et al.* Minfi: a flexible and comprehensive bioconductor package for the analysis of Infinium DNA methylation microarrays. *Bioinformatics* 2014; **30**: 1363–1369.
33. RStudio Team. *RStudio: Integrated Development for R*. RStudio, Inc: Boston, 2016. [Accessed 15 July 2021]. Available from: <http://www.rstudio.com/>
34. Pidsley R, Wong CCY, Volta M, *et al.* A data-driven approach to pre-processing Illumina 450K methylation array data. *BMC Genomics* 2013; **14**: 293.
35. Peters TJ, Buckley MJ, Statham AL, *et al.* *De novo* identification of differentially methylated regions in the human genome. *Epigenet Chromatin* 2015; **8**: 6.
36. Gu Z, Eils R, Schlesner M. Complex heatmaps reveal patterns and correlations in multidimensional genomic data. *Bioinformatics* 2016; **32**: 2847–2849.
37. Hovestadt V, Zapatka M. conumee: Enhanced copy-number variation analysis using Illumina DNA methylation arrays. R package version 1.9.0. [Accessed 15 July 2021]. Available from: <http://bioconductor.org/packages/conumee/>
38. Capper D, Stichel D, Sahm F, *et al.* Practical implementation of DNA methylation and copy-number-based CNS tumor diagnostics: the Heidelberg experience. *Acta Neuropathol* 2018; **136**: 181–210.
39. Krijgsman O, Carvalho B, Meijer GA, *et al.* Focal chromosomal copy number aberrations in cancer – needles in a genome haystack. *Biochim Biophys Acta* 1843; **2014**: 2698–2704.
40. Durinck S, Moreau Y, Kasprzyk A, *et al.* BioMart and Bioconductor: a powerful link between biological databases and microarray data analysis. *Bioinformatics* 2005; **21**: 3439–3440.
41. Durinck S, Spellman PT, Birney E, *et al.* Mapping identifiers for the integration of genomic datasets with the R/Bioconductor package biomaRt. *Nat Protoc* 2009; **4**: 1184–1191.
42. Sondka Z, Bamford S, Cole CG, *et al.* The COSMIC Cancer Gene Census: describing genetic dysfunction across all human cancers. *Nat Rev Cancer* 2018; **18**: 696–705.
43. Sullivan RJ, Infante JR, Janku F, *et al.* First-in-class ERK1/2 inhibitor ulixertinib (BVD-523) in patients with MAPK mutant advanced solid tumors: results of a phase I dose-escalation and expansion study. *Cancer Discov* 2018; **8**: 184–195.
44. Mazieres J, Cropet C, Montané L, *et al.* Vemurafenib in non-small-cell lung cancer patients with BRAF<sup>V600</sup> and BRAF<sup>nonV600</sup> mutations. *Ann Oncol* 2020; **31**: 289–294.
45. Beadling C, Jacobson-Dunlop E, Hodi FS, *et al.* KIT gene mutations and copy number in melanoma subtypes. *Clin Cancer Res* 2008; **14**: 6821–6828.
46. Furney SJ, Turajlic S, Stamp G, *et al.* Genome sequencing of mucosal melanomas reveals that they are driven by distinct mechanisms from cutaneous melanoma. *J Pathol* 2013; **230**: 261–269.
47. Xu L, Cheng Z, Cui C, *et al.* Frequent genetic aberrations in the cell cycle related genes in mucosal melanoma indicate the potential for targeted therapy. *J Transl Med* 2019; **17**: 245.
48. Zhou R, Shi C, Tao W, *et al.* Analysis of mucosal melanoma whole-genome landscapes reveals clinically relevant genomic aberrations. *Clin Cancer Res* 2019; **25**: 3548–3560.
49. Lyu J, Miao Y, Yu F, *et al.* CDK4 and TERT amplification in head and neck mucosal melanoma. *J Oral Pathol Med* 2021; **50**: 971–978.
50. Tang B, Sheng X, Kong Y, *et al.* Palbociclib for treatment of metastatic melanoma with copy number variations of CDK4 pathway: case report. *Chin Clin Oncol* 2018; **7**: 62.
51. Hoon DSB, Spugnardi M, Kuo C, *et al.* Profiling epigenetic inactivation of tumor suppressor genes in tumors and plasma from cutaneous melanoma patients. *Oncogene* 2004; **23**: 4014–4022.
52. Spugnardi M, Tommasi S, Dammann R, *et al.* Epigenetic inactivation of RAS association domain family protein 1 (RASSF1A) in malignant cutaneous melanoma. *Cancer Res* 2003; **63**: 1639–1643.
53. Straume O, Smeds J, Kumar R, *et al.* Significant impact of promoter hypermethylation and the 540 C>T polymorphism of CDKN2A in cutaneous melanoma of the vertical growth phase. *Am J Pathol* 2002; **161**: 229–237.
54. Moulin AP, Clément G, Bosman FT, *et al.* Methylation of CpG island promoters in uveal melanoma. *Br J Ophthalmol* 2008; **92**: 281–285.
55. Maat W, van der Velden PA, Out-Luiting C, *et al.* Epigenetic inactivation of RASSF1a in uveal melanoma. *Invest Ophthalmol Vis Sci* 2007; **48**: 486–490.
56. Field MG, Kuznetsov JN, Bussies PL, *et al.* BAP1 loss is associated with DNA methylomic repatterning in highly aggressive class 2 uveal melanomas. *Clin Cancer Res* 2019; **25**: 5663–5673.
57. Robertson AG, Shih J, Yau C, *et al.* Integrative analysis identifies four molecular and clinical subsets in uveal melanoma. *Cancer Cell* 2017; **32**: 204–220.e15.
58. Ferrier ST, Burnier JV. Novel methylation patterns predict outcome in uveal melanoma. *Life (Basel)* 2020; **10**: 248.
59. Lee SH, Roh MR, Kang B, *et al.* PTEN methylation dependent sinonasal mucosal melanoma. *Cancer Res Treat* 2016; **48**: 853–858.

## SUPPLEMENTARY MATERIAL ONLINE

**Figure S1.** Summary copy number plots showing the frequency of copy number alterations across different anatomic sites

**Figure S2.** Uniform manifold approximation and projection (UMAP) as well as t-distributed stochastic neighbor embedding (t-SNE) as dimensionality reduction methods to uncover similarities and differences between samples

**Figure S3.** Detailed investigation of the 1000 most significantly differentially methylated positions

**Figure S4.** Results from gene set enrichment analysis

**Table S1.** Clinical and histopathological metadata for the patients and tumor specimens that have been included in this study

**Table S2.** List of the genes and the respective exons covered by the next generation sequencing panel

**Table S3.** List of somatic mutations